

When are the $q/3$ fractional quantum Hall states stable?

Yang Liu, J. Shabani, and M. Shayegan

Department of Electrical Engineering, Princeton University, Princeton, New Jersey 08544

(Dated: June 29, 2021)

Magneto-transport measurements in a wide GaAs quantum well in which we can tune the Fermi energy (E_F) to lie in different Landau levels of the two occupied electric subbands reveal a remarkable pattern for the appearance and disappearance of fractional quantum Hall states at $\nu = 10/3, 11/3, 13/3, 14/3, 16/3$, and $17/3$. The data provide direct evidence that the $q/3$ states are stable and strong even at such high fillings as long as E_F lies in a ground-state ($N = 0$) Landau level of either of the two electric subbands, regardless of whether that level belongs to the symmetric or the anti-symmetric subband. Evidently, the node in the out-of-plane direction of the anti-symmetric subband does not de-stabilize the $q/3$ fractional states. On the other hand, when E_F lies in an excited ($N > 0$) Landau level of either subband, the wavefunction node(s) in the in-plane direction weaken or completely de-stabilize the $q/3$ fractional quantum Hall states. Our data also show that the $q/3$ states remain stable very near the crossing of two Landau levels belonging to the two subbands, especially if the levels have parallel spins.

I. INTRODUCTION

The fractional quantum Hall (FQH) effect,¹ signaled by the vanishing of the longitudinal resistance and the quantization of the Hall resistance, is the hallmark of an interacting two-dimensional electron system (2DES) in a large perpendicular magnetic field. It is a unique incompressible quantum liquid phase described by the celebrated Laughlin wavefunction.² In a standard, single-subband 2DES confined to a low-disorder GaAs quantum well, the FQH effect is most prominently observed at low Landau level (LL) filling factors $\nu < 2$, where the Fermi energy (E_F) lies in the spin-resolved LLs with the lowest orbital index ($N = 0$).³ The strongest states are seen at the $q/3$ fractional fillings, namely at $\nu = 1/3, 2/3, 4/3$, and $5/3$. In contrast, as illustrated in Fig. 1(a), when E_F lies in the second ($N = 1$) set of LLs ($2 < \nu < 4$), the equivalent $q/3$ states at $\nu = 7/3, 8/3, 10/3$, and $11/3$ are much weaker.^{4,5} In yet higher LLs ($\nu > 4$), e.g., at $\nu = 13/3, 14/3, 16/3$, and $17/3$, which correspond to E_F being in the third ($N = 2$) set of LLs, the FQH states are essentially absent;^{6–8} see Fig. 1(a). This absence is believed to be a result of the larger extent of the electron wavefunction (in the 2D plane) and its extra nodes that modify the (exchange-correlation) interaction effects and favor the stability of various non-uniform charge density states (e.g., stripe phases) over the FQH states.^{9–13}

Recently, the FQH effect was examined in a wide GaAs quantum well where two electric subbands are occupied.¹⁴ A main finding of Ref. 14 is highlighted in Fig. 1(b): When the Fermi level (E_F) lies in the $N = 0$ LLs of the anti-symmetric electric subband, the even-denominator FQH states (at $\nu = 5/2$ and $7/2$) are absent and, instead, strong FQH states are observed at $q/3$ fillings $\nu = 7/3, 8/3, 10/3$ and $11/3$. Here we extend the measurements in this two-subband system and examine the stability of the $q/3$ FQH states at even higher fillings as we tune the position of E_F to lie in different LLs of the two subbands. At a fixed 2DES density, we observe a remarkable pattern of alternating appearance and disap-

pearance of the $q/3$ states as we tune the subband separation and the position of E_F . The data demonstrate that the $q/3$ states are stable even at filling factors as high as $\nu = 17/3$, as long as E_F lies in a ground state ($N = 0$) LL, regardless of whether that LL belongs to the symmetric or anti-symmetric subband.

II. SAMPLE AND EXPERIMENTAL DETAILS

Our sample, grown by molecular beam epitaxy, is a 55 nm-wide GaAs quantum well (QW) bounded on each side by undoped $\text{Al}_{0.24}\text{Ga}_{0.76}\text{As}$ spacer layers and Si δ -doped layers.¹⁵ We fitted the sample with an evaporated Ti/Au front-gate and an In back-gate to change the 2D electron density, n , and tune the charge distribution symmetry and the occupancy of the two electric subbands, as demonstrated in Fig. 2. This tunability, combined with the very high mobility ($\sim 400 \text{ m}^2/\text{Vs}$) of the sample, is key to our success in probing the strength of the $q/3$ states at high fillings.

When the QW in our experiments is "balanced", i.e., the charge distribution is symmetric, the occupied subbands are the symmetric (S) and anti-symmetric (A) states (see the lower panels in Figs. 2(a) and (b)). When the QW is "imbalanced," the two occupied subbands are no longer symmetric or anti-symmetric; nevertheless, for brevity, we still refer to these as S (ground state) and A (excited state). In our experiments, we carefully control the electron density and charge distribution symmetry in the QW via applying back- and front-gate biases.^{16,17} For each pair of gate biases, we measure the occupied subband electron densities from the Fourier transforms of the low-field ($B \leq 0.5 \text{ T}$) Shubnikov-de Haas oscillations. These Fourier transforms, examples of which are shown in Fig. 2(c), exhibit two peaks (B_S and B_A) whose frequencies, multiplied by $2e/h$, give the subband densities, n_S and n_A . The difference between these densities directly gives the subband separation, Δ , through the expression $\Delta = \frac{\pi\hbar^2}{m^*}(n_S - n_A)$, where m^* is the electron

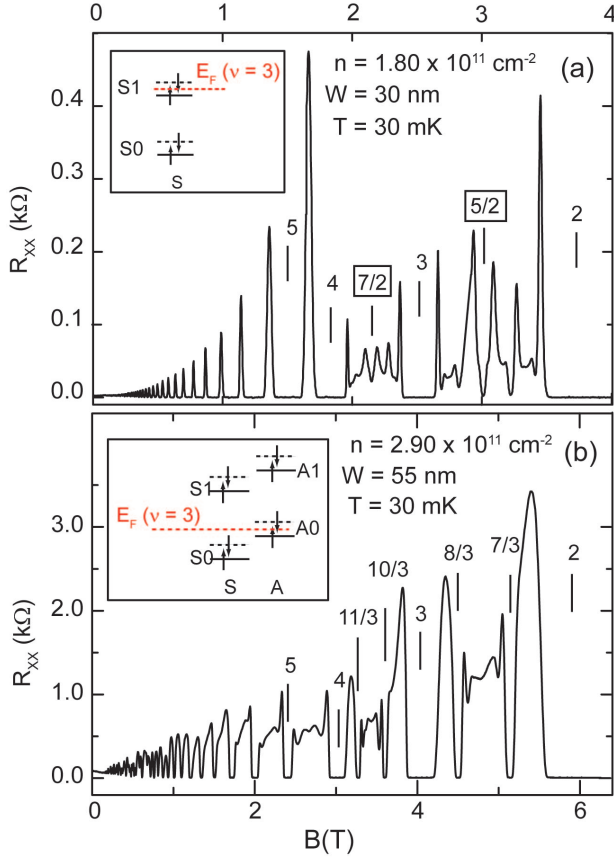


FIG. 1. Longitudinal resistance (R_{xx}) vs. perpendicular magnetic field (B) traces are shown for electrons confined to: (a) a narrow (well-width $W = 30$ nm) GaAs quantum well, and (b) a wide ($W = 55$ nm) quantum well. In (a) FQH states at $\nu = 5/2$ and $7/2$ can be clearly seen, but the states at $\nu = 7/3$ and $8/3$ are weak. In contrast, the even-denominator states are absent in (b) but strong FQH states are seen at $\nu = 7/3$ and $8/3$. Note also the absence of FQH states for $\nu > 4$ in (a). The insets schematically show the positions of the spin-split LLs of the lowest (S) and second (A) electric subbands, as well as the position of E_F at $\nu = 3$; the indices $N = 0$ and $N = 1$ indicate the lowest and the excited LLs, respectively. The subband separation for the trace in (b) is $\Delta = 24$ K.

effective mass. Note that, at a fixed total density, Δ is smallest when the charge distribution is balanced and it increases as the QW is imbalanced. Figure 2(d) shows the measured Δ as a function of the charge δn transferred between the back and front sides of the QW. Note that we measure δn from the change in the sample density induced by the application of either the back-gate or the front-gate bias.

III. MAGNETO-TRANSPORT DATA

Figure 3 shows a series of longitudinal resistance (R_{xx}) vs. magnetic field (B) traces taken at a fixed density

$n = 2.12 \times 10^{11} \text{ cm}^{-2}$ as the subband spacing is increased. The y-axis is Δ , which is measured from the low-field Shubnikov-de Haas oscillations of each trace. The same data are interpolated and presented in a color-scale plot in Fig. 4(a). In Fig. 5, we show a color-scale plot of the data in the low field regime.

In Figs. 3, 4(a), and 5 we observe numerous LL coincidences at various integer filling factors, signaled by a weakening or disappearance of the R_{xx} minimum. For example, the R_{xx} minimum at $\nu = 4$ is strong and wide at all values of Δ except near $\Delta = 32$ and 58 K, marked by squares in Fig. 4(a), where it becomes narrow or disappears. Such coincidences can be easily explained in a simple fan diagram of the LL energies in our system as a function of increasing Δ , as schematically shown in Fig. 4(b). In this figure, we denote an energy level by its subband index (S or A), LL index ($N = 0, 1, 2, \dots$), and spin (\uparrow or \downarrow). Also indicated in Fig. 4(b) are the separations between various levels: the cyclotron energy ($E_C = \hbar e B / m^*$), Zeeman energy ($E_Z = g^* \mu_B B$, where g^* is the effective Landé g-factor), and Δ . From Fig. 4(b) it is clear that the condition for observing a LL coincidence at odd fillings is $\Delta = i E_C$, while for coincidences at even fillings, the condition is $\Delta = i E_C \pm E_Z$; in both cases, i is a positive integer.

In Figs. 4(a) and 4(b), we have indicated the two coincidences at $\nu = 4$ with squares. Note that the coincidences at even fillings correspond to a crossing of two levels with antiparallel spins. In Figs. 3 and 4(a), the coincidences at low, odd fillings (e.g., $\nu = 3$ and 5) are not as easy to see at low temperatures since the resistance minima remain strong as the two LLs, which have parallel spins, cross. Such behavior has been reported previously and has been interpreted as a signature of easy-plane ferromagnetism.^{18–20} We note that our data taken at higher temperatures ($T = 0.31$ K) reveal a weakening of the $\nu = 5$ minimum at $\Delta = 35$ K, and of the $\nu = 3$ minimum at $\Delta = 58$ K;²¹ these are marked by circles in Fig. 4(a). The crossings at higher odd fillings are clearly seen in Figs. 4(a) and 5; e.g., the $\nu = 7$ minimum disappears at around $\Delta = 50$ K, and $\nu = 9$ around $\Delta = 40$ K and 60 K.²²

In Figs. 4(a) and 5 we include several solid white lines representing $\Delta = i E_C$, assuming GaAs band effective mass of $m^* = 0.067$ (in units of free electron mass). These lines indeed pass through the positions of the observed LL coincidences for odd fillings, implying that Δ is not re-normalized at LL coincidences. We note that, with the application of magnetic field, the subband electron occupation might vary because of the finite number of discrete LLs that are occupied. This could lead to a redistribution of charge which in turn could lead to changes in Δ as a function of magnetic field. At LL coincidences, however, the two crossing LLs which belong to the different subbands are energetically degenerate. If the coincidence occurs at the Fermi energy, electrons can move between the two degenerate LLs so that the subband occupancy and the charge distribution, and there-

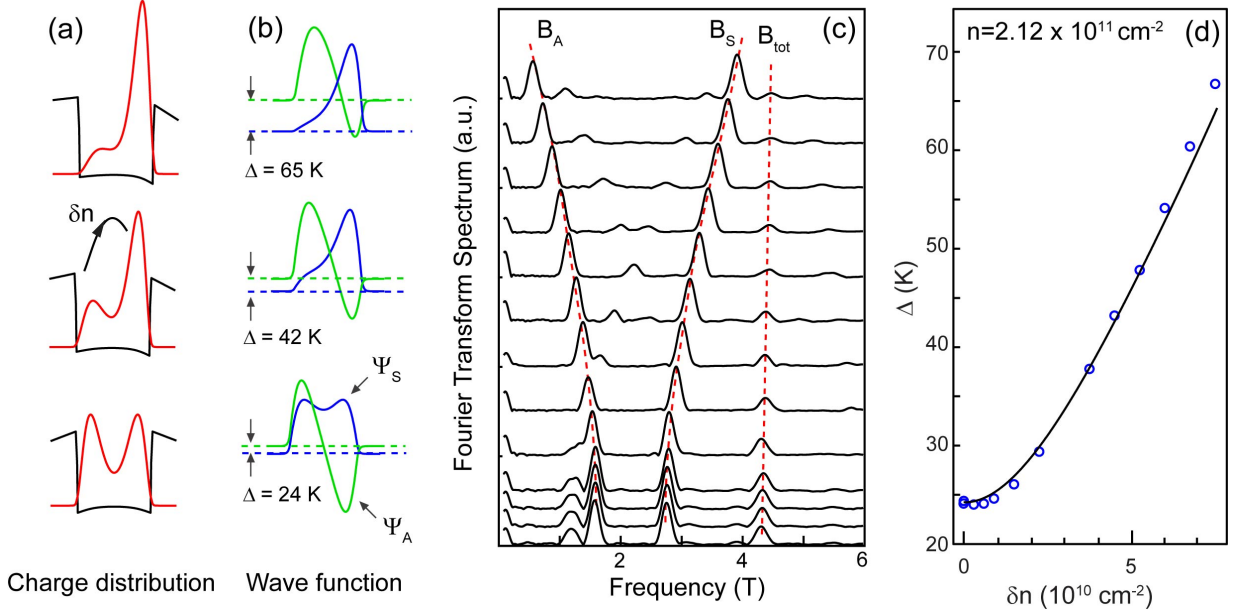


FIG. 2. (a) Charge distribution (red) and potential (black), and (b) wave functions from self-consistent simulations for a 55 nm-wide GaAs QW. The charge density is kept fixed at $n = 2.12 \times 10^{11} \text{ cm}^{-2}$. The subband separation Δ is the smallest when the QW is balanced (bottom panels), and increases as the QW is imbalanced. (c) The Fourier transform spectra of the measured low-field Shubnikov-de Haas oscillations. Each spectrum exhibits two main peaks, denoted as B_A and B_S , whose separation increases as the QW is imbalanced (from bottom to top). (d) The subband separation Δ determined from the Fourier transforms through $\Delta = \frac{\hbar e}{m^*} (B_S - B_A)$, plotted as a function of the charge distribution asymmetry δn . The solid curve represents Δ vs. δn from self-consistent calculations for a 55 nm-wide GaAs QW.

fore Δ , are restored back to their zero-field values. This conjecture is indeed confirmed by self-consistent calculations reported for a two-subband 2D electron system in a perpendicular magnetic field.²³ While the subband occupancy and Δ oscillate with field, they equal their zero-field values whenever two LLs belonging to different subbands coincide at E_F . We conclude that the field positions of the LL coincidences at E_F are determined by the value of Δ at $B = 0$, and that the lines drawn in Figs. 4(a) and 5 accurately describe the positions of these coincidences.

The dashed lines in Figs. 4(a) and 5, represent $\Delta = iE_C \pm E_Z$, $i = 1, 2, \dots$, where g^* is chosen as a fitting parameter so that these lines pass through the even-filling coincidences. All the dashed lines in Figs. 4(a) and 5 are drawn using $g^* = 8.8$, except for the $\Delta = E_C \pm E_Z$ lines, which are drawn using $g^* = 8.9$ and 7.6 , respectively. We conclude that g^* is enhanced by a factor of ~ 20 relative to the GaAs band g -factor (0.44). This enhancement is somewhat larger than the values reported for GaAs QWs with two subbands occupied. For example, Muraki *et al.*¹⁹ reported a ~ 10 -fold enhancement of g^* for electrons in a 40 nm-wide QW with $n \sim 3 \times 10^{11} \text{ cm}^{-2}$ while Zhang *et al.*²⁴ measured a ~ 5 -fold enhancement in a 24 nm-wide QW with $n \sim 7 \times 10^{11} \text{ cm}^{-2}$. It appears then that the enhancement depends on the QW width and electron density, and a systematic study of the enhancement would be an interesting future project.

However, we would like to emphasize that the dashed lines in Figs. 4(a) and 5 pass through nearly all of the observed coincidences quite well. Since each of these lines are drawn using very similar g^* , the data imply that the enhancement is nearly independent of the filling factor.²⁵

We now focus on the main finding of our work, namely the correspondence between the stability of the FQH states and the position of E_F . Note in Figs. 3 and 4(a) that FQH states are observed only in certain ranges of Δ . For example, the $\nu = 10/3$ and $11/3$ states are seen in the regions marked by A and C in Fig. 4(a) but they are essentially absent in the B region. The $\nu = 13/3$ and $14/3$ states, on the other hand, are absent in regions D and F while they are clearly seen in regions E and G.

To understand this behavior, in the fan diagram of Fig. 4(b) we have highlighted the position of E_F as a function of Δ for different filling factors by color-coded lines. Concentrating on the range $3 < \nu < 4$ (green line in Fig. 4(b)), at small values of Δ (region A), E_F lies in the $A0\downarrow$ level. At higher Δ , past the first $\nu = 4$ coincidence which occurs when $\Delta = E_C - E_Z$, E_F is in the $S1\uparrow$ level (region B). Once Δ exceeds E_C , E_F lies in the $A0\uparrow$ level (region C) until the second $\nu = 4$ coincidence occurs when $\Delta = E_C + E_Z$. Note in Fig. 4(a) that strong FQH states at $\nu = 10/3$ and $11/3$ are seen in regions A and C. From the fan diagram of Fig. 4(b) it is clear that in these regions E_F is in the *ground-state* ($N = 0$) LLs of the asymmetric subband, i.e., $A0\uparrow$

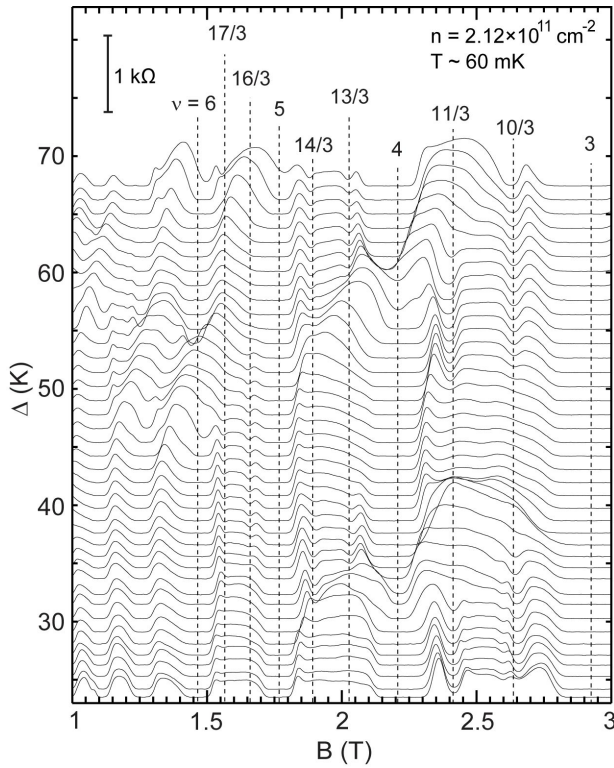


FIG. 3. Waterfall plot of R_{xx} vs. B taken at a fixed density $n = 2.12 \times 10^{11} \text{ cm}^{-2}$ as the subband separation (Δ) is increased. The scale for R_{xx} is indicated in the upper left (0 to 1 k Ω). Each trace is shifted vertically so that its zero (of R_{xx}) is aligned with its measured value of Δ which is used as the y-axis of the waterfall plot. Vertical lines mark the field positions of the filling factors, ν .

and $A0\downarrow$. In contrast, in region B, where the $10/3$ and $11/3$ states are essentially absent, E_F lies in an *excited* ($N = 1$) LL, namely, $S1\uparrow$. We conclude that the $10/3$ and $11/3$ FQH states are stable and strong when E_F lies in a ground-state LL.

The data in the range $4 < \nu < 5$ corroborate the above conclusion. In Fig. 4(b) we represent the position of E_F in this filling range by a blue line. In regions E and G, E_F lies in the ground-state LLs of the asymmetric subband ($A0\downarrow$ and $A0\uparrow$), and these regions are indeed where the $\nu = 13/3$ and $14/3$ FQH states are seen. In regions D and F, on the other hand, E_F is in the excited LLs of the symmetric subband ($S1\uparrow$ and $S1\downarrow$), and the $13/3$ and $14/3$ FQH states are absent. Data at yet higher fillings ($5 < \nu < 6$) follow the same trend: FQH states at $\nu = 16/3$ and $17/3$ are seen in region I when E_F is in the $A0\downarrow$ level,²⁶ but they are absent in regions H or J where E_F lies in the $S1\downarrow$ or $S2\uparrow$ levels.

In Fig. 6 we show additional data for a density of $n = 2.90 \times 10^{11} \text{ cm}^{-2}$ in the same QW. Longitudinal and Hall resistance traces are shown in the bottom panels for three different values of Δ , and in each panel the calculated charge distribution (at $B = 0$) is also shown. In the top panels, we show the positions of the LLs and

E_F , corresponding to the filling factors in the bottom panels. In all cases, strong $q/3$ FQH states are observed when E_F lies in the $N = 0$ of the $A0\downarrow$ level. Note that the data shown in Fig. 6 are for asymmetric charge distributions. We would like to emphasize that strong $q/3$ states are also observed for symmetric ("balanced") charge distributions; e.g., see the bottom trace in Fig. 3, or the traces in Fig. 2(c) of Shabani *et al.*¹⁴

Next we address the FQH states observed at lower ν (< 3) in our sample. Data are shown for $n = 2.12 \times 10^{11} \text{ cm}^{-2}$ for the "balanced" QW ($\Delta = 23 \text{ K}$) in Fig. 7; the R_{xx} trace is an extension of the lowest trace shown in Fig. 3. In the range $1 < \nu < 3$, strong FQH states are seen at $\nu = 4/3, 5/3, 7/3$ and $8/3$. Data taken at yet higher magnetic fields (not shown) reveal the presence of a very strong FQH state at $\nu = 2/3$. From the fan diagram of Fig. 4(b), it is clear that E_F at these fillings lies in an $N = 0$ LL, namely, the $A0\uparrow$ ($\nu = 7/3$ and $8/3$), $S0\downarrow$ ($\nu = 4/3$ and $5/3$), or $S0\uparrow$ ($\nu = 2/3$) levels.²⁷

IV. DISCUSSION

Our observations provide direct evidence that the $q/3$ FQH states are strong when E_F resides in a ground-state ($N = 0$) LL, regardless of whether that LL belongs to the A or S subband. This finding implies that the node in the wavefunction in the *out-of-plane* direction does not significantly de-stabilize the $q/3$ FQH states. On the other hand, when E_F lies in an $N > 0$ LL, the wavefunction node(s) in the *in-plane* direction weaken or completely de-stabilize the $q/3$ FQH states. These conclusions are consistent with the data from single-subband samples,^{4,6-8} as well as theoretical calculations.^{5,9-13} In a composite Fermion picture, our data also imply that the lower lying (fully occupied) LLs are essentially inert and the composite Fermions are formed in the partially filled LL where E_F lies. The composite Fermions, however, could have a spin and/or subband degree of freedom, as we briefly discuss in the last paragraph of this section (see also, Ref. 14).

Our data also allow us to assess the stability of the FQH states as two LLs approach each other. In Fig. 4(a) the dashed line denoted $E_C - E_Z$ marks the position of the expected crossing between the $A0\downarrow$ and the $S1\uparrow$ levels, based on the LL coincidence we observe for the $\nu = 4$ quantum Hall state. It is clear in Fig. 4(a) that as we approach this line from the A region, the $10/3$ and $11/3$ FQH states disappear when Δ is about 5 K away from $E_C - E_Z$. A similar statement can be made regarding the stability of the $11/3$ state as the $E_C + E_Z$ dashed line is approached from the C region, and the stability of the $13/3$ and $14/3$ states as one approaches the $E_C + E_Z$ line from the G region or the $E_C - E_Z$ line from the E region.²⁶ Note that what is common to all these observations is that the boundaries marked by the dashed lines correspond to the crossing of two LLs with *antiparallel* spins.

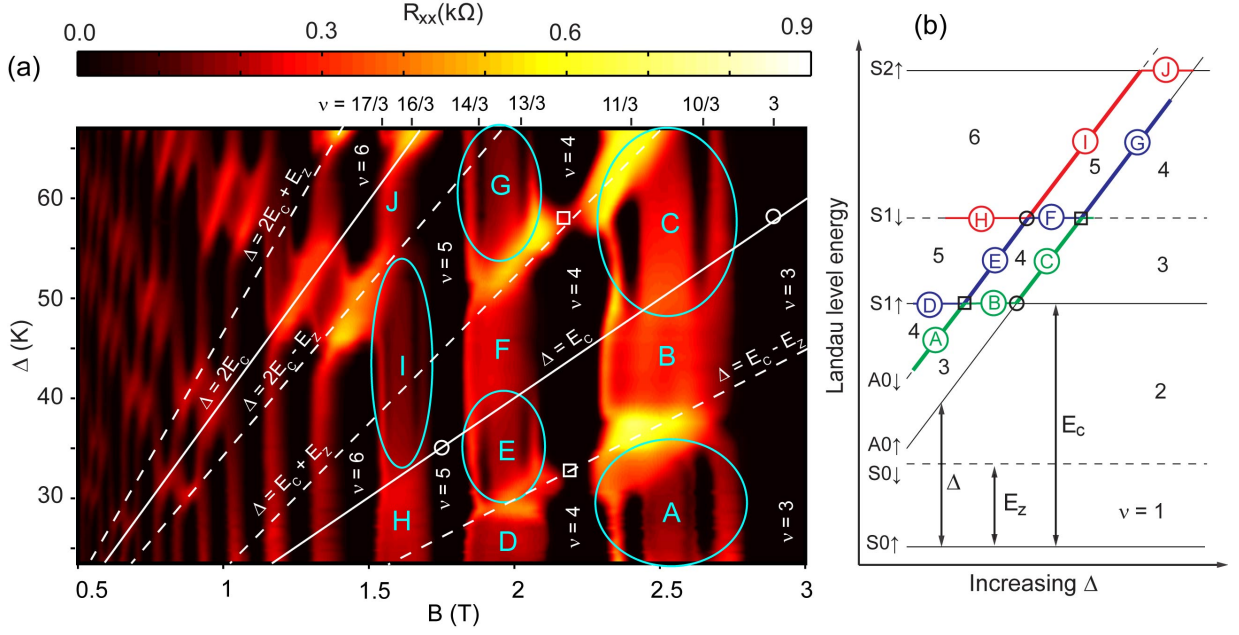


FIG. 4. Evolution of R_{xx} data taken at a fixed density $n = 2.12 \times 10^{11} \text{ cm}^{-2}$ as the subband separation (Δ) is increased. (a) A color-scale plot of the data shown in Fig. 3. The dark regions are where the integer or fractional quantum Hall states are observed at the indicated values of ν . The solid white lines denote $\Delta = E_C$ and $\Delta = 2E_C$, where E_C is the cyclotron energy. The dashed white lines are drawn such that they pass through the even-filling coincidences (see text). The cyan ellipses mark different regions (A, C, E, G, and I) where FQH states are seen. (b) Schematic electron Landau level diagram as a function of increasing Δ . The relevant energies, Δ , the cyclotron energy (E_C), and the Zeeman energy (E_Z), are shown. The position of the Fermi level is plotted in different colors for several filling factor regions: $3 < \nu < 4$ (green), $4 < \nu < 5$ (blue), and $5 < \nu < 6$ (red). The letters correspond to the regions in the (a) panel; the regions where FQH states are observed are marked by thicker lines.

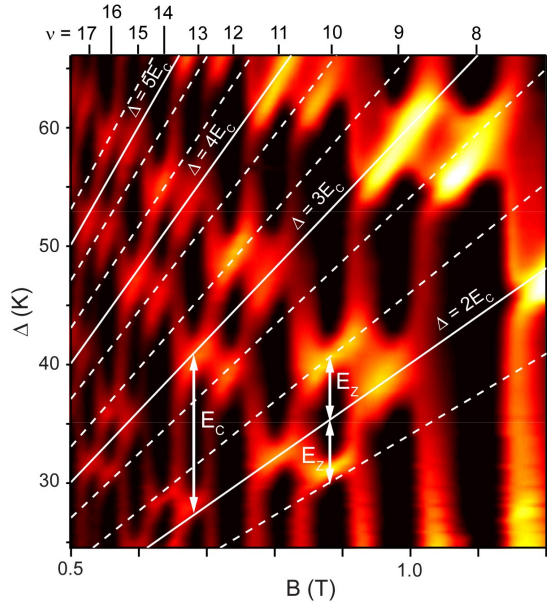


FIG. 5. An expanded color-scale plot of R_{xx} data at low fields for $n = 2.12 \times 10^{11} \text{ cm}^{-2}$. The solid white lines denote $\Delta = iE_C$ for $i = 2, 3, 4, 5$. The dashed white lines represent $\Delta = iE_C \pm E_Z$, using a fixed $g^* = 8.8$ (see text).

Data of Fig. 4(a) suggest that, when the two approaching LLs have *parallel* spins, the $q/3$ states remain stable even closer to the expected LL crossings. For example, the $10/3$ and $11/3$ FQH states in region C are stable very close to the boundary (the line marked E_C) separating this region from B. Similarly, the $13/3$ and $14/3$ states are stable in region E close to the E_C line separating E from F. Note that in both cases, i.e., traversing from C to B or from E to F, the two approaching LLs have parallel spins (see Fig. 4(b)). We conclude that the relative spins of the two approaching LLs also play a role in the stability of the $q/3$ FQH states. It is worth emphasizing that, as is evident from Figs. 3 and 4(a) data, the relative spins of the two approaching LLs also play a crucial role in the stability of the *integer* quantum Hall (IQH) states. For antiparallel-spin LLs, the IQH state (e.g., at $\nu = 4$) becomes very weak or completely disappears, while for the parallel-spin LLs the IQH state (e.g., at $\nu = 3$), remains strong. This behavior has been attributed to easy-axis (for an opposite-spin crossing) and easy-plane (for a same-spin crossing) ferromagnetism.^{18–20}

We highlight three further observations. First, strong FQH states at large $q/3$ fillings have been recently observed in very high quality graphene samples.²⁸ These states qualitatively resemble what we see in our two-subband system. It is tempting to associate the valley

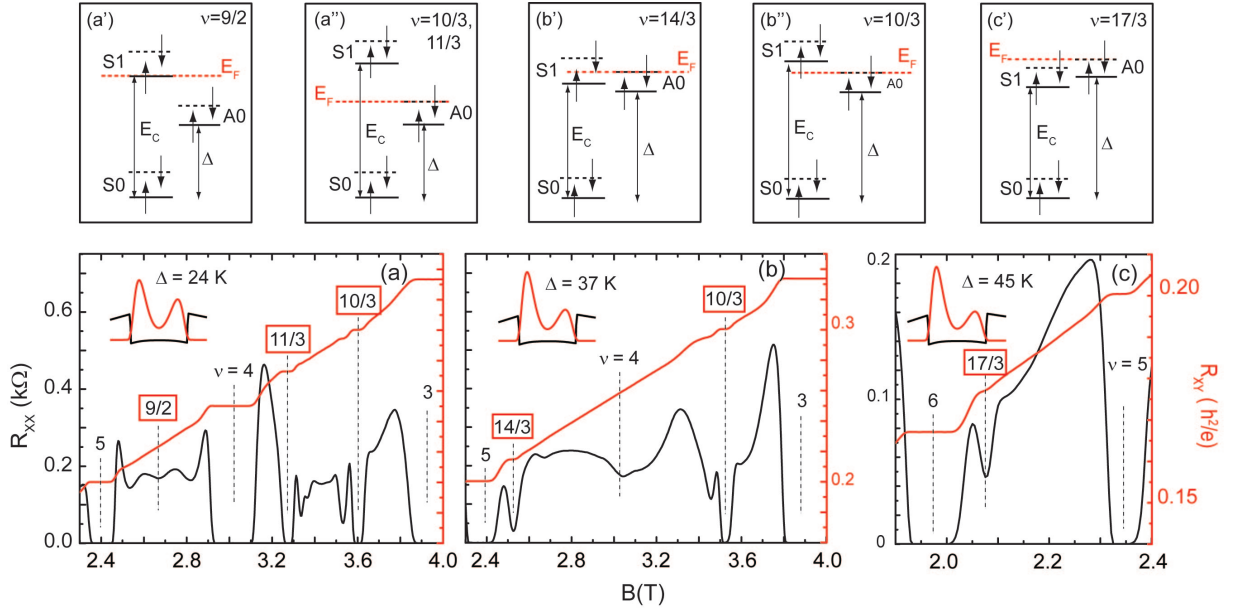


FIG. 6. (a), (b), (c) Longitudinal (R_{xx}) and Hall (R_{xy}) resistances for the 55 nm-wide QW at a higher density $n = 2.90 \times 10^{11} \text{ cm}^{-2}$. Panels (a) and (b) share the same scales for R_{xx} and R_{xy} . The traces were taken at $T = 30 \text{ mK}$, and the insets show the charge distributions calculated at $B = 0$. The LL diagrams for fractional fillings in panels (a), (b) and (c) are shown in (a'), (a''), (b') and (b''), and (c'), respectively. Fractional quantum Hall states at $\nu = 10/3, 11/3, 14/3$, and $17/3$ are clearly seen when E_F lies in either the $A0\uparrow$ or $A0\downarrow$ levels.

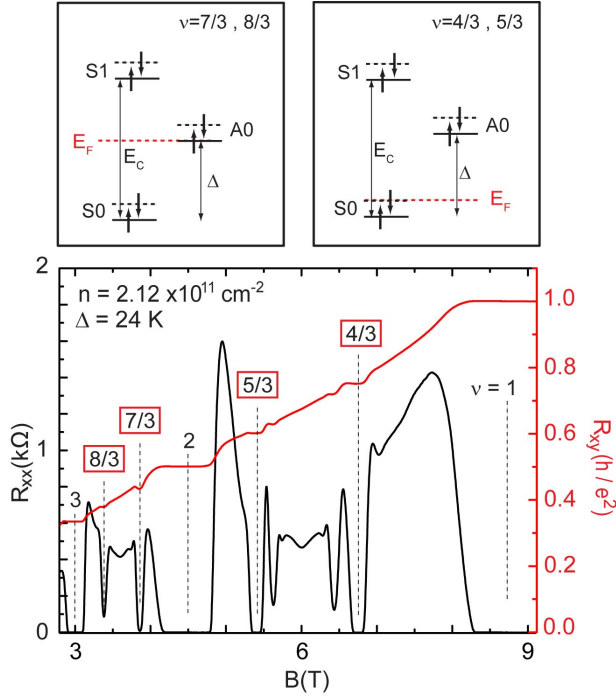


FIG. 7. R_{xx} and R_{xy} traces at high magnetic fields and $T = 30 \text{ mK}$ for $n = 2.12 \times 10^{11} \text{ cm}^{-2}$ for the "balanced" QW. Fractional quantum Hall states at $\nu = 4/3, 5/3, 7/3$, and $8/3$ are clearly seen. The upper panels show the LL diagrams and positions of E_F for the indicated fillings.

degree of freedom in graphene with the subband degree of freedom in our sample. But the LL structure in graphene is of course different from GaAs so it is not obvious if this association is valid. Second, data taken in the $N = 1$ LL at very low temperatures and in the highest quality, single-subband samples exhibit FQH states at even-denominator fillings $\nu = 5/2$ and $7/2$.^{29,30} In the traces shown in Fig. 3, we do not see any even-denominator states when $N = 1$, e.g., at $\nu = 7/2$ in region B where E_F is in the $S1\uparrow$ level. However, in the same sample, at higher densities ($n > 3.4 \times 10^{11} \text{ cm}^{-2}$) and at low temperatures ($T = 30 \text{ mK}$), we do indeed observe a FQH state at $\nu = 7/2$ flanked by very weak $10/3$ and $11/3$ states when E_F lies in the $S1\uparrow$ level.¹⁴

Third, in the $N = 0$ LL, high-quality samples show strong higher-order, odd-denominator FQH states at composite Fermion filling factor sequences such as $2/5, 3/7, 4/9$, etc.³ We do observe a qualitatively similar behavior in our data when E_F is in an $N = 0$ LL. For example, in region A (Figs. 3 and 4(a)) we see weak but clear minima at $\nu = 17/5$ next to the $10/3$ minimum. Again, at higher densities and low temperatures, such states become more developed.¹⁴ In Fig. 1(b), for example, there are strong minima at $\nu = 12/5$ and $13/5$, adjacent to the $7/3$ and $8/3$ minima, and at $17/5$ and $18/5$, adjacent to the $10/3$ and $11/3$ minima. These states, as well as the $q/3$ states, exhibit subtle evolutions even when E_F lies within a fixed $N = 0$ LL, consistent with the presence of composite Fermions which have spin and/or subband degrees of freedom.¹⁴ A related question concerns the role of charge distribution symmetry in the stability of the $q/3$

states. In other words, in a QW with fixed width, density and filling, and with E_F in a particular $N = 0$ LL, how does the strength of given a FQH state at a particular filling vary with charge distribution symmetry. We do not have data to answer this question quantitatively, but the data we present here clearly indicates that a primary factor determining the strength of the $q/3$ FQH states is whether or not E_F lies in an $N = 0$ LL.

V. SUMMARY

In conclusion, the position of E_F is what determines the stability of odd-denominator, $q/3$ FQH states at a given filling factor. When E_F lies in a ground-state ($N = 0$) LL, the $q/3$ FQH states are stable and strong,

regardless of whether that LL belongs to the symmetric or antisymmetric subband. This observation implies that the wavefunction node in the out-of-plane direction is not detrimental to the stability of these FQH states. Also, the $q/3$ FQH states appear to be stable very near the crossing of two LLs, especially if the LLs have parallel spins.

ACKNOWLEDGMENTS

We acknowledge support through the NSF (DMR-0904117 and MRSEC DMR-0819860) for sample fabrication and characterization, and the DOE BES (DE-FG0200-ER45841) for measurements. We thank J. K. Jain and Z. Papic for illuminating discussions.

-
- ¹ D. C. Tsui, H. L. Stormer, and A. C. Gossard, Phys. Rev. Lett. **48**, 1559 (1982).
 - ² R. B. Laughlin, Phys. Rev. Lett. **50**, 1395 (1983).
 - ³ J. K. Jain, *Composite Fermions* (Cambridge University Press, New York, 2007).
 - ⁴ W. Pan, J.-S. Xia, V. Shvarts, D. E. Adams, H. L. Stormer, D. C. Tsui, L. N. Pfeiffer, K. W. Baldwin, and K. W. West, Phys. Rev. Lett. **83**, 3530 (1999).
 - ⁵ C. Töke, M. R. Peterson, G. S. Jeon, and J. K. Jain, Phys. Rev. B **72**, 125315 (2005).
 - ⁶ M. P. Lilly, K. B. Cooper, J. P. Eisenstein, L. N. Pfeiffer, and K. W. West, Phys. Rev. Lett. **82**, 394 (1999).
 - ⁷ R. Du, D. Tsui, H. Stormer, L. Pfeiffer, K. Baldwin, and K. West, Solid State Communications **109**, 389 (1999).
 - ⁸ G. Gervais, L. W. Engel, H. L. Stormer, D. C. Tsui, K. W. Baldwin, K. W. West, and L. N. Pfeiffer, Phys. Rev. Lett. **93**, 266804 (2004).
 - ⁹ F. D. M. Haldane, *The quantum Hall effect*, edited by R. E. Prange and S. M. Girvin (Springer, New York, 1987) pp. 303–352.
 - ¹⁰ A. H. MacDonald and S. M. Girvin, Phys. Rev. B **33**, 4009 (1986).
 - ¹¹ N. d’Ambrumenil and A. Reynolds, Journal of Physics C: Solid State Physics **21**, 119 (1988).
 - ¹² A. A. Koulakov, M. M. Fogler, and B. I. Shklovskii, Phys. Rev. Lett. **76**, 499 (1996).
 - ¹³ R. Moessner and J. T. Chalker, Phys. Rev. B **54**, 5006 (1996).
 - ¹⁴ J. Shabani, Y. Liu, and M. Shayegan, Phys. Rev. Lett. **105**, 246805 (2010).
 - ¹⁵ Our sample is the same as the one used in Ref. 14. Based on our careful measurements of the subband separation (Δ) while imbalancing the QW (see Fig. 2), we conclude that the QW has a width of 55 nm, slightly smaller than 56 nm which was quoted in Ref. 14. We emphasize that throughout our paper we use the experimentally measured values of Δ , and that the exact width of the QW has no bearing on our conclusions.
 - ¹⁶ Y. W. Suen, H. C. Manoharan, X. Ying, M. B. Santos, and M. Shayegan, Phys. Rev. Lett. **72**, 3405 (1994).
 - ¹⁷ J. Shabani, T. Gokmen, Y. T. Chiu, and M. Shayegan, Phys. Rev. Lett. **103**, 256802 (2009).
 - ¹⁸ T. Jungwirth, S. P. Shukla, L. Smrčka, M. Shayegan, and A. H. MacDonald, Phys. Rev. Lett. **81**, 2328 (1998).
 - ¹⁹ K. Muraki, T. Saku, and Y. Hirayama, Phys. Rev. Lett. **87**, 196801 (2001).
 - ²⁰ K. Vakili, T. Gokmen, O. Gunawan, Y. P. Shkolnikov, E. P. De Poortere, and M. Shayegan, Phys. Rev. Lett. **97**, 116803 (2006).
 - ²¹ J. Shabani, Ph.D. thesis, Princeton University (2011).
 - ²² We note that when the charge distribution is nearly symmetric, LL coincidences at even fillings are also difficult to see at very low temperatures. For example, there is a coincidence at $\nu = 8$ at $\Delta \simeq 26$ K but we can only see a weakening of the R_{xx} minimum at $T \gtrsim 0.3$ K.
 - ²³ S. Trott, G. Paasch, G. Gobsch, and M. Trott, Phys. Rev. B **39**, 10232 (1989).
 - ²⁴ X. C. Zhang, I. Martin, and H. W. Jiang, Phys. Rev. B **74**, 073301 (2006).
 - ²⁵ The observation of a significantly enhanced g-factor which is independent of the filling factor has been reported in the past [S. J. Papadakis, E. P. De Poortere, and M. Shayegan, Phys. Rev. B **59**, R12743 (1999); Y. P. Shkolnikov, E. P. De Poortere, E. Tutuc, and M. Shayegan, Phys. Rev. Lett. **89**, 226805 (2002)].
 - ²⁶ The $E_C + E_Z$ line going through region I does not correspond to a LL coincidence at the Fermi energy in this region; this should be evident from Fig. 4(b) diagram. The same is true about the $2E_C - E_Z$ line as it goes through region G.
 - ²⁷ Traces taken at higher values of Δ reveal that the $\nu = 7/3$ and $8/3$ states remain strong up to the $\nu = 3$ coincidence. Past this coincidence, the $7/3$ and $8/3$ states become weaker, consistent with the fact that E_F now lies in an excited LL (the $S1\uparrow$ level, see Fig. 4(b)).
 - ²⁸ C. R. Dean, A. F. Young, P. Cadden-Zimansky, L. Wang, H. Ren, K. Watanabe, T. Taniguchi, P. Kim, J. Hone, and K. L. Shepard, arXiv:1010.1179 (2010).
 - ²⁹ R. Willett, J. P. Eisenstein, H. L. Störmer, D. C. Tsui, A. C. Gossard, and J. H. English, Phys. Rev. Lett. **59**, 1776 (1987).
 - ³⁰ W. Pan, J. S. Xia, H. L. Stormer, D. C. Tsui, C. Vicente, E. D. Adams, N. S. Sullivan, L. N. Pfeiffer, K. W. Baldwin, and K. W. West, Phys. Rev. B **77**, 075307 (2008).